

pubs.acs.org/JPCA Article

A Shock-Tube Study of the Rate Constant of $PH_3 + M \rightleftharpoons PH_2 + H + M$ (M = Ar) Using PH_3 Laser Absorption

Clayton R. Mulvihill,* Raquel Juárez, Olivier Mathieu, and Eric L. Petersen



Cite This: J. Phys. Chem. A 2020, 124, 7380-7387



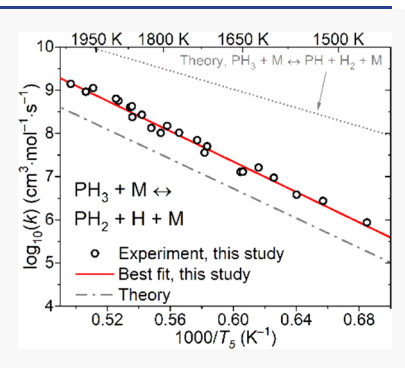
ACCESS

Metrics & More



Supporting Information

ABSTRACT: Phosphine (PH₃) is a highly reactive and toxic gas. Prior experimental investigations of PH₃ pyrolysis reactions have included only low-temperature measurements. This study reports the first shock-tube measurements of PH₃ pyrolysis using a new PH₃ laser absorption technique near $4.56 \, \mu \text{m}$. Experiments were conducted in mixtures of $0.5\% \, \text{PH}_3/\text{A}$ and reflected shock waves at temperatures of $1460-2013 \, \text{K}$ and pressures of $\sim 1.3 \, \text{and}$ $\sim 0.5 \, \text{atm}$. The PH₃ time histories displayed two-stage behavior similar to that previously observed for NH₃ decomposition, suggesting by analogy that the rate constant for PH₃ + M $\rightleftharpoons \text{PH}_2 + \text{H} + \text{M}$ (R1) could be determined. A simple three-step mechanism was assembled for data analysis. In a detailed kinetic analysis of the first-stage PH₃ decomposition, values of $k_{1,0}$ were obtained and best described by (in cm³·mol⁻¹·s⁻¹) $k_{1,0} = 7.78 \times 10^{17} \, \text{exp}(-80,400/RT)$, with units of cal, mol, K, s, and cm³. Agreement between the 1.3 and 0.5 atm data confirmed that the measured $k_{1,0}$ was in the low-pressure limit. Agreement of the



experimental $k_{1,0}$ with ab initio estimates resolved the question of the main pathway of PH₃ decomposition: it proceeds as PH₃ \rightleftarrows PH₂ + H instead of PH₃ \rightleftarrows PH + H₂.

1. INTRODUCTION

Phosphine (PH₃) is a toxic¹ and pyrophoric² gas that is used as a phosphorus source in the semiconductor industry^{3,4} and as a fumigant in the agricultural industry.¹ A recent focus on phosphorous chemistry has arisen out of an interest in organophosphorus compounds (OPCs), which can serve as both fire suppressants⁵ and surrogates for chemical weapons of mass destruction such as Sarin.⁶ Although PH₃ is not an OPC, its small size and correspondingly simple chemistry may make it suitable as a foundation for more-complex phosphorous chemistry and as a precursor for various phosphorus-containing intermediates.

The pyrolysis kinetics of PH3 have received only a handful of studies. The title reaction, $PH_3 \rightleftharpoons PH_2 + H$, has been studied theoretically via RRKM calculations by Buchan and Jasinski³ and by Cardelino et al.4 However, no experimental data appear to exist on this reaction, and even the pathway by which PH3 decomposition proceeds was still unclear in the opinion of Buchan and Jasinski (see Section 4.1). The secondary reaction in studied theoretically via various direct dynamics ab initio methods by Yu et al. The reaction $PH_3 + H \rightleftharpoons PH_2 + H_2$ has also been studied in several experimental works.⁸⁻¹⁰ Lee et al. measured H atom levels during flash photolysis of PH₃/He mixtures from 209 to 495 K.8 Aleksandrov et al. measured H and P atoms during a flow-discharge experiment involving H₂ and PH₃ in He at room temperature. Finally, Arthur and Cooper measured H atoms during flash photolysis of PH₃/H₂/Hg mixtures from 293 to 472 K.¹⁰ The results of these three experimental studies are all in good agreement. However, these

experiments were performed only at low temperatures (209–495 K).

To rectify the lack of experimental data on the title reaction and on high-temperature PH_3 pyrolysis, this study provides the first measurement of the PH_3 decomposition rate constant, $k_{1,0}$, and the first high-temperature experimental data involving PH_3 . Described first is the experiment, including the development of a new PH_3 laser absorption diagnostic. Experimental PH_3 profiles are then provided, followed by the method used to extract the decomposition rate constant. Comparisons to previous theoretical studies of PH_3 decomposition are made, and conclusions concerning future directions of PH_3 mechanism development are drawn.

2. EXPERIMENT

2.1. Shock Tube. A single-diaphragm shock tube was used for all experiments. The 10.8 cm-square driven section was 4.0 m long, while the 7.6 cm-diameter driver was 2.0 m long. Polycarbonate diaphragms (0.127 mm in thickness) were burst using He as the driver gas for the 1.3 atm experiments and a mixture of He and air for the 0.5 atm experiments. Mechanical and turbomolecular pumps achieved ultimate

Received: June 2, 2020 Revised: August 19, 2020 Published: September 2, 2020





driven-section pressures of $\sim 10^{-8}$ atm before each experiment. Four piezoelectric pressure transducers along the last 1.4 m of the driven section measured the incident shock wave velocity, $\nu_{\rm s}$. The linear attenuation of v_s was extrapolated to the endwall and used with known initial conditions (T_1 and P_1) to calculate the temperature (T_5) and pressure (P_5) behind the reflected shock wave (RSW) using the 1D normal shock relations. Estimated uncertainties in T_5 and P_5 are ± 0.8 and $\pm 1.0\%$, respectively.

PH₃ was supplied by Praxair as a 0.5% PH₃/Ar mixture with a relative PH3 uncertainty of ±2%. Stated purity levels were 99.9997% for PH₃ and 99.9999% for Ar. The PH₃/Ar mixture was filled directly into the driven section prior to each experiment. Since NH3 is known to adsorb onto stainless steel, it was suspected that PH3 may experience a similar phenomenon. To prevent this adsorption, a two-stage filling/ vacuuming passivation method similar to that of Mathieu and Petersen¹ was utilized, although this was likely unnecessary as it appears PH₃ does not strongly adsorb onto stainless steel. ¹² Due to the highly dangerous nature of PH3, enhanced safety precautions were taken while handling PH3: (i) a negativepressure cabinet was used to store the PH₃/Ar bottle, (ii) PH₃ detectors were stationed throughout the laboratory, and (iii) gas lines were filled with PH₃/Ar to only slightly above atmospheric pressure to minimize the risk of PH₃ leaks while still preventing air infiltration.

A thin layer of red powder accumulated near the shock-tube endwall after repeated PH3 pyrolysis experiments. Chemical equilibrium calculations were performed using thermodynamic data from Burcat and Ruscic¹³ for Ar, H, H₂, P, P₂, PH, PH₂, PH₃, P₂H, P₂H₂, and P₂H₄. These calculations indicated that the stable products of PH₃/Ar mixtures at high temperatures were predominantly P2, H2, and Ar. Thus, the red powder was almost certainly red phosphorus. Additionally, the chemical equilibrium calculations indicated the equilibrium PH3 mole fraction was ~1 \times 10⁻⁸, which confirmed the experimentally observed disappearance of PH3 at higher temperatures where the shocktube test time was sufficiently long to fully observe this disappearance (Section 3.1).

2.2. Laser Diagnostic. A quantum cascade laser (Alpes Lasers) generated narrow-linewidth ($\sim 5 \times 10^{-5}$ cm⁻¹) light near 2193 cm⁻¹. A beam splitter directed incident (I_0) and transmitted (I_t) portions of the beam onto either of two InSb, 200 kHz-bandwidth photodetectors (Teledyne Judson J10D); time histories were accordingly postprocessed with a 200 kHzcutoff digital filter. The It beam traversed two CaF2 shock-tube window ports located 1 cm from the endwall. Irises and bandpass filters were successfully employed to eliminate broadband emission interference: an experiment with the laser turned off revealed no broadband emission being captured by the It detector during pyrolysis of 0.5% PH3/Ar at the hightemperature end of this study. A flip mirror directed the laser into a wavemeter (Bristol 671B-MIR) to monitor the laser frequency. For more details on the laser hardware, see Mulvihill et al.14

Representative experimental results are shown in Figure 1 in the form of a laser transmission trace (Figure 1a) and a sidewall pressure trace (Figure 1b). The sidewall pressure trace was taken from the piezoelectric transducer in the same plane as the CaF₂ windows. In Figure 1a, PH3 absorption can be observed before and after the incident shock wave since PH3 is absorbed at this wavelength at room temperature. (The identical transmission levels before the incident shock wave and after the RSW are merely fortuitous; Section 3.3 shows a case where this agreement

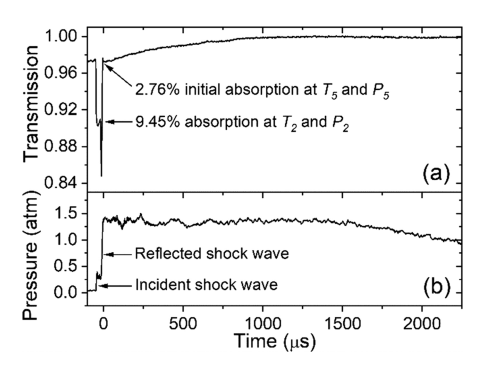


Figure 1. Representative (a) laser transmission and (b) sidewall pressure traces in a mixture of 0.5% PH₃/Ar at 1719 K, 1.37 atm. The laser transmission is defined as $I_{\rm t}/I_{\rm 0}$. The laser frequency was fixed at 2192.771 cm⁻¹ for this experiment. The value of k_v for this experiment was calculated to be 0.377 cm⁻¹·atm⁻¹.

does not occur.) Following the passage of the RSW, PH3 absorption begins to decrease as the PH3 decomposes. During all PH₃ pyrolysis experiments, the laser frequency was fixed at 2192.771 ± 0.001 cm⁻¹ (see Section 2.3 for more on the determination of this frequency).

The Beer–Lambert law, $I_t/I_0 = \exp(-k_v P X_{abs} L)$, was utilized to process the experimental I_t/I_0 time histories. The pressure P was P_5 , while L was 10.8 cm. The initial PH₃ concentration (0.5%) was used as the mole fraction of the absorbing species, X_{abst} along with the measured initial absorption behind the RSW (e.g., 2.76% in Figure 1a) to derive the absorption coefficient, k_v , which was held constant when processing the experimental transmission profiles via the Beer-Lambert law to obtain PH₃ time histories. Although k_y is a function of T_5 and P_5 (see Figure S14 in the Supporting Information), the PH₃ time histories were self-calibrating due to the known initial concentration of PH₃.

2.3. Spectroscopic Characterization of PH₃. PH₃ exhibits strong absorption in the 4-5 μ m range due to the v_1 , $2\nu_2$, ν_3 , ν_2 + ν_4 , and $2\nu_4$ bands. This region is the strongest region of PH3 absorption in the IR. The selected wavelength (2192.77 cm⁻¹) is one of the strongest transitions in this region at high temperatures (1500-2000 K) and was chosen due to the tuning range of the available quantum cascade laser. Roomtemperature, scanned-wavelength measurements of PH3 were performed near 2192 cm⁻¹ by modulating the laser injection current at 100 Hz to achieve a scanning range of ~1 cm⁻¹. A 50.8-mm, solid germanium etalon with a free spectral range of 0.024 cm⁻¹ monitored relative changes in the laser frequency, while the wavemeter ascertained the absolute frequency. Experimental and calculated room-temperature spectra are shown in Figure 2a,b, respectively.

In Figure 2, the line positions of the HITRAN2016 database and of the data are observed to typically have discrepancies of about ± 0.01 cm⁻¹, which is near the standard error of ± 0.009 cm⁻¹ reported by the measurements¹⁵ that HITRAN2016 cites. However, HITRAN2016 incorrectly predicts the frequency of the strong line observed experimentally at 2192.771 cm⁻¹ by nearly 0.1 cm⁻¹. HITRAN2016 identifies the strong transition at 2192.6737 cm⁻¹ as the $15_{14} \leftarrow 16_{15}$ line in the 0010 \leftarrow 0000 band but labels the symmetry species as "A" even though it should be either "A+" or "A-" (alternatively, " A_1 " or " A_2 "). 15 This ambiguity in labeling may be related to the error in line position predicted by HITRAN2016. Despite this error in the HITRAN2016 prediction, the strong transition at 2192.771

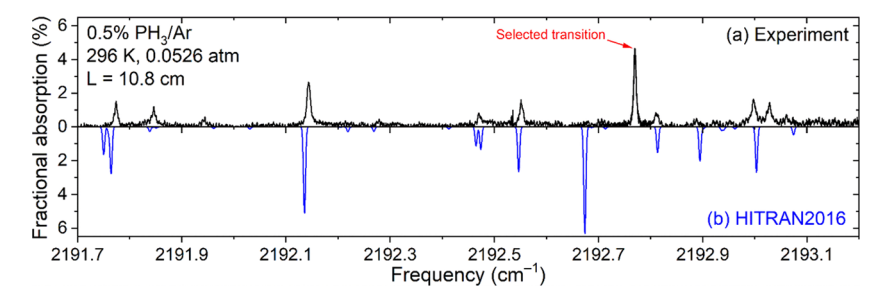


Figure 2. (a) Measured and (b) predicted room-temperature spectra of PH₃ near 2192 cm⁻¹. The experimental data comprise two overlapping scans. Predictions were calculated using line positions, line strengths, and partition functions from the HITRAN2016 database¹⁶ and assumed a PH₃–Ar broadening coefficient of 0.045 cm⁻¹·atm⁻¹, which is the average value from Dhib et al. ¹⁷ for NH₃–Ar broadening in the ν_4 band.

cm⁻¹ is still suitable for use in the fixed-wavelength experiments, as discussed later.

As an additional confirmation that the experimentally observed transition at 2192.771 cm⁻¹ was the same as that predicted by HITRAN2016 at 2192.6737 cm⁻¹, the room-temperature line strength of this transition was assessed using the experimental data in Figure 2. A best-fit Voigt profile to the Figure 2 data for the transition at 2192.771 cm⁻¹ yielded a line strength of 0.117 cm⁻²·atm⁻¹. In comparison, the HITRAN2016 line strength at 296 K for the transition at 2192.6737 cm⁻¹ is 0.1133 cm⁻²·atm⁻¹. The close agreement (3.2%) between the two line strengths strongly suggests that the two transitions are the same and that the HITRAN2016 line position is simply incorrect.

To investigate the high-temperature spectra of the strong PH₃ transition near 2192.771 cm⁻¹, scanned-wavelength tests were performed behind the RSW. Due to the limited test time available behind the RSW, the laser injection current was modulated at a higher speed (2 kHz) for these RSW experiments; a smaller scan range (~0.5 cm⁻¹) was obtained due to the higher modulation frequency. Relatively cold temperatures were chosen for these RSW experiments to reduce PH₃ decomposition during the scan time. Sample results from a scanned-wavelength measurement behind the RSW are shown in Figure 3. Compared to the data shown in Figure 2, the hightemperature and high-pressure data in Figure 3 demonstrate (i) weaker absorption features (on a per-column-density basis) due to the redistribution of molecules to higher energy levels at the higher temperature, (ii) more absorption features due to the population of higher energy levels at the higher temperature, and (iii) broader absorption features due to stronger collisional broadening at the higher pressure. Also shown in Figure 3 is a

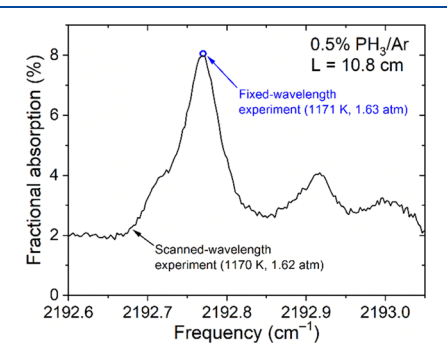


Figure 3. High-temperature PH_3 spectra near 2192.7 cm⁻¹ obtained during a scanned-wavelength experiment behind the RSW. The open circle denotes a fixed-wavelength experiment at nearly identical test conditions.

single, fixed-wavelength experiment at nearly the same $T_{\rm S}$ and $P_{\rm S}$ as the scanned-wavelength experiment wherein the laser frequency was fixed at 2192.771 cm⁻¹. The peak absorption for this fixed-wavelength experiment (8.05%) was obtained immediately behind the RSW (cf. the value of 2.76% in Figure 1a). The excellent agreement between the fixed- and scanned-wavelength measurements in Figure 3 supports the accuracy of both techniques. Since HITRAN2016 only contains air-broadening coefficients for PH₃, it is difficult to directly compare the predictions of HITRAN2016 with the $k_{\rm v}$ data shown in Figure S14. However, by employing the assumption of a constant Ar-to-air broadening coefficient and considering the fixed-wavelength $k_{\rm v}$ data shown in Figure S14, the authors roughly estimate an Ar-to-air broadening coefficient ratio of 0.4 for the strong PH₃ transition at 2192.771 cm⁻¹.

The goal of the brief spectroscopic characterization illustrated in Figures 2 and 3 was not to fully characterize the PH₃ absorption spectrum in this region; such a task goes beyond the scope of this work. Instead, the goal of the spectroscopic characterization was to identify a frequency at which to fix the laser to obtain the maximum possible fractional absorption by PH₃ for the PH₃ pyrolysis experiments. Based on Figures 2 and 3, the laser frequency was fixed at the center (2192.771 \pm 0.001 cm⁻¹) of the strong transition in Figures 2 and 3 for all pyrolysis experiments herein. The minimum resolvable fractional absorption was ~0.07%, yielding a PH₃ detection limit of ~110 ppm.

3. RESULTS

3.1. PH₃ Time Histories. Representative PH₃ time histories across a range of temperatures at a pressure of \sim 1.3 atm are shown in Figure 4. Each profile exhibited a first stage of PH₃ decomposition, lasting $50-100 \, \mu s$, followed by a second stage of

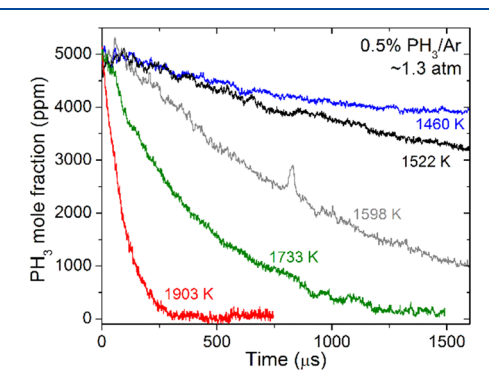


Figure 4. PH_3 decomposition profiles in 0.5% PH_3/Ar at various temperatures and an average pressure of 1.3 atm.

faster PH3 decomposition for the remainder of the experiment (the timescale in Figure 4 makes the two-stage behavior difficult to ascertain; see Sections 3.3 and 4.4 for further examples of the two-stage decomposition). The two-stage behavior was most evident at intermediate temperatures, becoming more difficult to discern at the temperature extrema of the present study. The difficulty in discerning the two-stage behavior at low temperatures was due to reduced PH3 decomposition during the experimental time frame; at high temperatures, this difficulty was due to the fact that the first-stage decomposition lasted for nearly the entire period of decomposition of PH3, as has been similarly observed for NH₃²⁰ It was initially suspected that the two-stage behavior was due to long vibrational relaxation times of the shock-heated PH₃. However, this suspicion was disproved in three ways: (i) low-temperature (\sim 1200 K) experiments, where vibrational relaxation times should be relatively larger, in PH₃/ Ar showed nearly instantaneous (i.e., less than the \sim 4 μ s obfuscation time caused by the RSW) vibrational relaxation; (ii) a high-temperature experiment in PH₃/Ar with 10% He (which accelerates vibrational relaxation) added to the mixture showed identical PH₃ decomposition behavior to the experiments without He; and (iii) the nitrogen analog to PH3, NH3, is known to have extremely short ($<0.1 \mu s$) vibrational relaxation times at the conditions of this study. 18 Based on these three arguments, vibrational relaxation was determined to be of no concern in the present experiments and not responsible for the observed two-stage PH3 decomposition.

To aid future modelers in studying the PH₃ pyrolysis system, a total of 13 PH₃ time histories have been provided in the Supporting Information at pressures of \sim 1.3 and \sim 0.5 atm.

3.2. Three-Step Pyrolysis Mechanism. To model and interpret the first stage of the experimental PH₃ decomposition data, a three-step reaction mechanism was assembled containing the following reactions:

$$PH_3 + M \rightleftharpoons PH_2 + H + M \tag{R1}$$

$$PH_3 + H \rightleftharpoons PH_2 + H_2 \tag{R2}$$

$$H_2 + M \rightleftharpoons H + H + M.$$
 (R3)

The choice of these reactions was guided by analogy to NH₃ decomposition; see the following paragraph. The Arrhenius parameters used to describe R1–R3 are given in Table 1. The thermochemical data for Ar, H, H₂, PH₂, and PH₃ were taken from Burcat and Ruscic. ¹³ Separate text files containing both the reaction set and the thermochemical data are provided in the Supporting Information to this paper.

Table 1. Three-Step Mechanism Used for Data Reduction^a

no.	reaction	A	n	$E_{\rm a}$ (cal/mol)	reference
1	$\begin{array}{c} \mathrm{PH_3} + \mathrm{M} \rightleftarrows \mathrm{PH_2} + \\ \mathrm{H} + \mathrm{M} \end{array}$	7.78×10^{17}	0	80,400	this study ^b
2	$PH_3 + H \rightleftharpoons PH_2 + H_2$	2.91×10^{6}	2.271	-200	7^c
3	$H_2 + M \rightleftharpoons H + H + M$	4.58×10^{19}	-1.400	104,400	19 ^d

 ^{a}k given as $k = AT^{n}\exp{(-E_{a}/RT)}$. Units are cal, mol, K, s, cm³. These are the final, best-fit Arrhenius parameters. $k_{1,0}$ was adjusted to best fit each individual experiment; see Section 3.3. ^cBest-fit to the CVT/SCT calculations of Yu et al., ⁷ see Figure 5. ^dUses the enhanced H₂ collider efficiency of 2.50 suggested by Tsang and Hampson. ¹⁹

The selection of R1, R2, and R3 should now be addressed. In Section 3.1, two-stage decomposition behavior in the experimental PH₃ time histories was mentioned (see Sections 3.3 and 4.4 for more examples). This two-stage behavior guided the selection of the R1 and R2: similar two-stage decomposition was previously observed during NH₃ pyrolysis experiments by Holzrichter and Wagner. Holzrichter and Wagner utilized the slope of the first \sim 200 μ s of their NH₃ decomposition profiles to derive the rate constant, $k_{4.0}$, of

$$NH_3 + M \rightleftharpoons NH_2 + H + M.$$
 (R4)

However, Davidson et al. 21 later demonstrated that neglecting the reaction

$$NH_3 + H \rightleftharpoons NH_2 + H_2 \tag{R5}$$

in the analysis of NH₃ pyrolysis data, as Holzrichter and Wagner did, can lead to misinterpretations of $k_{4,0}$. When Davidson et al. accounted for k_5 in the determination of $k_{4,0}$, reinterpreted $k_{4,0}$ data from several groups coalesced to within 15% of one another. Therefore, given the resemblance of the PH₃ decomposition time histories obtained in this study to NH₃ time histories obtained in previous studies (e.g., ref 20), it seemed reasonable to model the first-stage decomposition of PH₃ using the phosphorous analogs of R4 and R5, that is, R1 and R2, respectively. The reaction R3 was included in the three-step mechanism for completeness; see Section 4.3 for more on this. Since R1 represents the low-pressure limit of unimolecular PH₃ decomposition, the corresponding rate constant will be referred to as $k_{1,0}$ (see Section 4.2 for more on $k_{1,0}$ and the high-pressure limit rate constant, $k_{1,\infty}$).

The rate constant for R2 was taken from Yu et al.,⁷ who calculated k_2 using transition state theory (TST) and canonical variational TST both with (CVT/SCT) and without (CVT) a tunneling correction. The CVT/SCT results were selected here as they most closely matched the low-temperature (200–500 K) experimental data of Lee et al.⁸ and Arthur and Cooper. ¹⁰ A three-parameter Arrhenius equation for k_2 was fit to the CVT/SCT results from Yu et al. (see the solid line in Figure 5) and is provided in Table 1.

3.3. Extraction of k_{1,0} **Data.** A kinetic analysis was performed in CHEMKIN PRO (closed homogeneous batch reactor, constant U-V) to match predictions of the three-step mechanism to experimental first-stage decomposition data by varying $k_{1,0}$. Using this method, a best-fit value of $k_{1,0}$ was determined for each individual PH₃ pyrolysis experiment; an

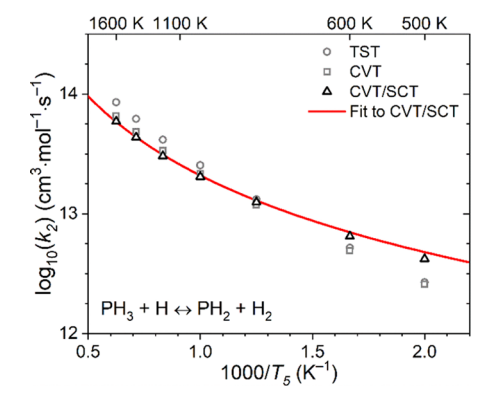


Figure 5. Arrhenius plot of k_2 . Symbols represent theoretical predictions from Yu et al., and the solid line represents three-parameter Arrhenius fit to the CVT/SCT predictions from Yu et al.

example is shown in Figure 6. An Arrhenius plot of the extracted $k_{1,0}$ values is shown in Figure 7. The 1.3 and 0.5 atm datasets are shown in Figure 7 and agree with each other within the scatter of the data. Using the $k_{1,0}$ data in Figure 7, a two-parameter Arrhenius expression for $k_{1,0}$ was fit to the experimental data and is given by $k_{1,0} = 7.78 \times 10^{17} \exp(-80,400/RT)$, with units of cal, mol, K, s, and cm³.

The previous NH₃ decomposition study by Holzrichter and Wagner²⁰ noted that the two-stage behavior became more difficult to discern at higher temperatures. Our results show similar trends; the hottest experiments shown in the Supporting Information demonstrate that the first-stage decomposition lasts for nearly the entire period of PH₃ decomposition. In discerning the inflection point where the first stage ended and the second stage began (e.g., $\sim 55~\mu s$ in Figure 6), it was useful to take the natural logarithm of the PH₃ mole fraction; a clear change in the slope of $\ln(X_{\rm PH_3})$ marked the inflection point; see Figure 6b for an example of this change in slope. However, it should be emphasized that a first-order analysis was not used to extract $k_{1,0}$; the three-step mechanism discussed in the preceding paragraphs was instead used.

4. DISCUSSION

4.1. Comparison with Theoretical Studies. There are only two previous studies of R1: the theoretical studies of Buchan and Jasinski³ and Cardelino et al.⁴ Both studies utilized RRKM theory to calculate the high-pressure-limit rate constant,

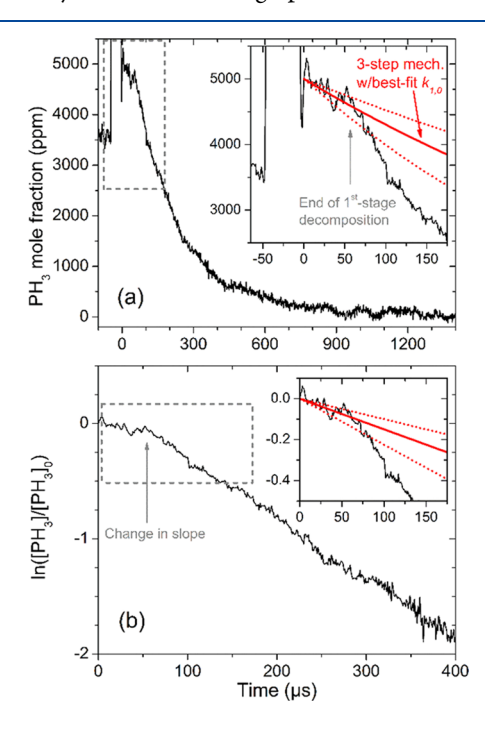


Figure 6. (a) PH₃ time history at 1805 K, 1.30 atm in 0.5% PH₃/Ar. The inset of panel (a) shows zoomed-in portion of the early experiment where the two-stage behavior is evident. (b) Natural logarithm of the normalized PH₃ mole fraction for the same experiment as shown in panel (a). The inset of panel (b) shows zoomed-in portion of the early experiment. The thick solid line represents prediction of the three-step mechanism using the best-fit $k_{1,0}$ for this experiment, 8.52×10^7 cm³· mol⁻¹·s⁻¹. Dotted lines represent mechanism predictions with $\pm 50\%$ variations in $k_{1,0}$. The fitting was only conducted up to the end of the first-stage decomposition, which is highlighted by the vertical arrow and is marked by a change of slope in panel (b).

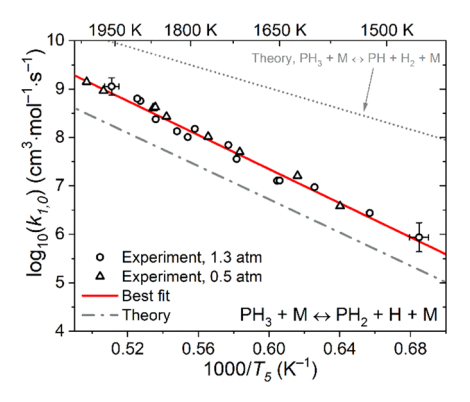


Figure 7. Arrhenius plot of $k_{1,0}$. Symbols represent individual experimental values of the current study. The solid line represents the current study's best-fit Arrhenius expression to the experimental data, $k_{1,0} = 7.78 \times 10^{17} \exp(-80,400/RT)$, with units of cal, mol, K, s, and cm³. The dash-dot line represents theoretical predictions for $k_{1,0}$ from Buchan and Jasinski.³ The dotted line represents theoretical predictions for the alternate pathway $PH_3 + M \rightleftharpoons PH + H_2 + M$ from Buchan and Jasinski.³

 $k_{1,\infty}$, of PH₃ unimolecular decomposition. The low-pressure-limit rate constant, $k_{1,0}$, was not explicitly provided by Buchan and Jasinski and had to be extracted. Using the fall-off curves shown in their Figure 1 for 700, 900, and 1100 K in conjunction with their value of $k_{1,\infty}$, expressions for $k_{1,0}$ were extracted and are provided in Table 2. The parameters for $k_{1,\infty}$ from Buchan and Jasinski are also included in Table 2. The Cardelino et al. values are not included in Table 2 since units and definitions were not clearly specified in their Table 3.

Buchan and Jasinski³ considered two possible reaction paths for PH₃ decomposition: PH₃ \rightleftharpoons PH₂ + H (pathway 1) and PH₃ \rightleftharpoons PH + H₂ (pathway 2). They concluded the more-important pathway was unclear and left the matter up for discussion. However, two new pieces of evidence now support pathway 1. First, Buchan and Jasinski's predicted $k_{1,0}$ of pathway 2 is ~200 and \sim 10 times higher than the experimental $k_{1,0}$ at the low- and high-temperature ends of this study; similarly, their predicted E_a for pathway 2 is \sim 32 kcal/mol lower than the experimental E_3 of this study (see the dotted line in Figure 7). The fact that the data analysis assumed pathway 1 did not significantly bias the measured $k_{1,0}$; at most, a factor-of-two increase in the experimental $k_{1,0}$ would have been obtained if pathway 2 had instead been assumed in the three-step mechanism. On the other hand, Buchan and Jasinski's calculated $k_{1,0}$ for pathway 1 is only ~ 4 times less than the experimental $k_{1,0}$, and their calculated E_a for pathway 1 is within 2 kcal/mol of the experimental E_a (see the dash-dot line in Figure 7). In summary, our measured $k_{1,0}$ is in much better agreement with Buchan and Jasinski's pathway 1 calculations than with their pathway 2 calculations. Second, the later study by Cardelino et al.4 considered only pathway 1, lending further support to the idea that PH₃ \rightleftarrows PH₂ + H is the preferred channel for PH₃ decomposition. Physically, the simultaneous removal of two H atoms to form H₂, as required by pathway 2, seems unlikely, and the loss of a single H atom (i.e., pathway 1) seems more plausible.

In extracting $k_{1,0}$ from Buchan and Jasinski,³ their eq 10 was used to correct their fall-off curves to an Ar bath gas to align with the experimental conditions of this study. The PH₃ collisional cross-section was taken from Svehla.²² Including this Ar bath gas correction, their $k_{1,0}$ expression is \sim 4 times lower than the

Table 2. Arrhenius Parameters of $k_{1,\infty}$ and $k_{1,0}$ via Two Different Pathways According to RRKM Calculations by Buchan and Jasinski^{3a}

	$k_{1,\infty}$		$k_{1,0}$			
reaction	$A (s^{-1})$	n	E _a (cal/mol)	$(cm^3 \cdot mol^{-1} \cdot s^{-1})$	n	E_a (cal/mol)
$PH_3 \rightleftharpoons PH_2 + H $ (pathway 1)	5.50 × 10 ¹⁵	0	82,500	1.00×10^{17}	0	78,367
$PH_3 \rightleftharpoons PH + H_2 $ (pathway 2)	1.51×10^{14}	0	53,100	2.76×10^{15}	0	48,960

"Pathway 2 is not valid; see text. The $k_{1,0}$ expressions given here are for M = Ar and were not explicitly stated by Buchan and Jasinski but rather extracted from their Figure 1. k is given as k = AT" exp $(-E_a/RT)$.

experimental $k_{1,0}$ determined in this study (see Figure 7). Buchan and Jasinski recommended a value of 0.1 for the collider efficiency, λ , of Ar relative to toluene. The extracted expression for $k_{1,0}$ is directly proportional to λ : if $\lambda = 0.2$ were used instead, the theoretical $k_{1,0}$ from Buchan and Jasinski increases by a factor of two.

4.2. Pressure Dependence of PH₃ **Decomposition.** In comparing against the $k_{1,0}$ predictions from Buchan and Jasinski,³ it was assumed that the present experimental conditions were within the low-pressure limit of PH₃ decomposition. Based on the agreement of our 1.3 and 0.5 atm experimental data, the present data did indeed assess the low-pressure limit.

Beside the fact that the current study was in the low-pressure limit, little else can be said about the pressure dependence of PH $_3$ decomposition. Neither Buchan and Jasinski 3 nor Cardelino et al. 4 seem to have addressed the fall-off behavior; their $k_{\rm l,uni}$ discussions or plots employed simple Lindemann fits. Based on the Buchan and Jasinski calculations using a Lindemann fit, the predicted fall-off pressure, $P_{\rm 1/2}$, was $\sim\!400$ atm at the conditions of this study, which is in general accord with the fact that the present study was in the low-pressure limit. Further work is needed on the fall-off behavior of PH $_3$ decomposition.

4.3. Uncertainty in $k_{1,0}$. Uncertainty in the Arrhenius expression for $k_{1,0}$ arises primarily from noise in the first-stage decomposition, particularly at lower temperatures. This uncertainty is illustrated by the dotted lines in Figure 6. Estimated fitting uncertainties are factors of 1.5 and 2 at the high- and low-temperature ends of this study, respectively. The other primary uncertainty source is T_5 ($\pm 0.8\%$), although this is included as an x-axis uncertainty in Figure 7.

The $k_{1,0}$ uncertainty introduced by uncertainty in k_2 is negligible. The inclusion of R2 in the three-step mechanism was quite necessary as excluding R2 entirely from the data analysis yielded $k_{1,0}$ values that were consistently double those shown in Figure 7. This apparent doubling of $k_{1,0}$ in the absence of R2 is in accord with the relative magnitudes of $k_{1,0}$ and k_2 : at the conditions of the present study, k_2 is 4–7 orders of magnitude larger than $k_{1,0}$. Therefore, each H atom that is produced by R1 is immediately consumed by R2 along with a PH₃ molecule; R2 thereby provides another pathway for PH₃ consumption. Consequently, if R2 were excluded from the mechanism, then $k_{1,0}$ would need to be twice as large to model the experimentally observed disappearance of PH₃. However, due to the orders-of-magnitude differences in $k_{1,0}$ and k_2 , the best-fit $k_{1,0}$ was quite

insensitive to changes in k_2 : factor-of-three variations in k_2 caused only ~0.2% changes in the best-fit values of $k_{1,0}$ for the hottest and coldest experiments in this study. Note that the preceding comments only pertain to the first-stage decomposition of PH₃ wherein $k_{1,0}$ was determined.

The $k_{1,0}$ uncertainty introduced by uncertainty in k_3 is also negligible. Indeed, the inclusion of R3 in the three-step mechanism was found to have no effect on the best-fit $k_{1,0}$; it was included in the analysis merely for the sake of completeness and could have been excluded with no ill effects.

4.4. Second-Stage PH₃ Decomposition. The three-step mechanism shown in Table 1 is only capable of modeling the first-stage PH₃ decomposition. For example, the three-step mechanism can accurately predict only the first $\sim\!60~\mu s$ of the experiment in Figure 8; past this inflection point, other reactions become more important (Figure 6 and its inset demonstrate similar behavior). Additionally, Figure 8 demonstrates that removing R2 from the three-step mechanism yields decomposition profiles that are too slow.

As mentioned previously, the two-stage PH₃ decomposition behavior noted in Figure 8 has been previously observed for NH₃ decomposition. Therefore, to tentatively identify key reactions for modeling the second-stage decomposition of PH₃, simulations of NH₃ decomposition were performed using the mechanism of Zhang et al.²³ Similar conditions to the present study were simulated (0.5% NH₃/Ar, 1 atm, 2000–2800 K). Higher temperatures were required for the simulations of NH₃ decomposition because the rate constant for NH₃ decomposition, $k_{4,0}$, is ~3 orders of magnitude smaller than that for $k_{1,0}$ at 1500–2500 K.

As expected, the simulated NH $_3$ profiles exhibited two-stage behavior similar to the experimental PH $_3$ profiles obtained herein. A sensitivity analysis based on the NH $_3$ concentration was conducted. Throughout the simulation time (2 ms), NH $_3$ + M \rightleftarrows NH $_2$ + H + M (R4) remained the most sensitive reaction. However, upon reaching second-stage consumption of NH $_3$, the second-most sensitive reaction became NH $_2$ + NH \rightleftarrows N $_2$ H $_2$ + H. The reactions NH + H \rightleftarrows N + H $_2$ and NH + N \rightleftarrows N $_2$ + H were also important during the second-stage decomposition. It may be assumed that the analogous phosphorous reactions would play key roles in explaining the second-stage decomposition of PH $_3$; future experimental or theoretical attention given to PH $_3$ pyrolysis may benefit from focusing on these three reactions.

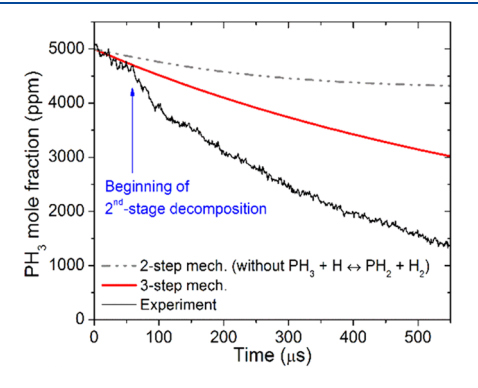


Figure 8. Experimental and modeled PH_3 decomposition at 1733 K, 1.32 atm in 0.5% PH_3/Ar . The thick solid line represents the mechanism of Table 1, and the dash-dot-dot line represents the mechanism of Table 1 with R2 removed.

The analogy to NH₃ decomposition was employed due to the dearth of rate constant data in the PH₃ system. As more knowledge on rate constants in the PH₃ decomposition system becomes available, an improved analysis of the most sensitive reactions during the second-stage decomposition may be possible.

5. CONCLUSIONS

A novel PH₃ laser absorption diagnostic near 2193 cm⁻¹ was developed and characterized. PH₃ time histories were acquired in PH₃/Ar mixtures behind reflected shock waves from 1460 to 2013 K at ~1.3 and ~0.5 atm. Using a three-step mechanism, $k_{1,0}$ was extracted for each individual experiment by inspecting the first-stage PH₃ decomposition. An Arrhenius expression was fit to the $k_{1,0}$ data. Agreement between the 1.3 and 0.5 atm data indicated the experimentally derived $k_{1,0}$ was indeed in the low-pressure limit. Agreement with the theoretical estimates of $k_{1,0}$ by Buchan and Jasinski³ confirmed the PH₃ decomposition pathway PH₃ \rightleftarrows PH₂ + H instead of the alternate pathway PH₃ \rightleftarrows PH + H₂.

The three-step mechanism was only able to describe the first-stage decomposition of PH₃, and further work is needed to improve the pyrolysis mechanism. The newly acquired data, provided in the Supporting Information, will facilitate such future improvements. By analogy to kinetics calculations of NH₃ pyrolysis, likely reactions that merit future attention are PH₂ + PH \rightleftarrows P₂H₂ + H, PH + H \rightleftarrows P + H₂, and PH + P \rightleftarrows P₂ + H. Investigation of these reactions will aid in the modeling of PH₃ oxidation, with applications to further understanding of OPC chemistry.

ASSOCIATED CONTENT

Supporting Information

The Supporting Information is available free of charge at https://pubs.acs.org/doi/10.1021/acs.jpca.0c04917.

Table of $k_{1,0}$ values, PH $_3$ time histories, and plot of $k_{\rm v}$ versus T_5 (PDF)

Three-step reaction mechanism in CHEMKIN format (TXT)

Thermochemical data for the three-step mechanism in CHEMKIN format (TXT)

AUTHOR INFORMATION

Corresponding Author

Clayton R. Mulvihill — J. Mike Walker '66 Department of Mechanical Engineering, Texas A&M University, College Station, Texas 77843, United States; Email: cmulvihill@tamu.edu

Authors

Raquel Juárez – J. Mike Walker '66 Department of Mechanical Engineering, Texas A&M University, College Station, Texas 77843, United States

Olivier Mathieu − *J. Mike Walker '66 Department of Mechanical Engineering, Texas A&M University, College Station, Texas 77843, United States;* orcid.org/0000-0002-8658-6326

Eric L. Petersen – J. Mike Walker '66 Department of Mechanical Engineering, Texas A&M University, College Station, Texas 77843, United States

Complete contact information is available at: https://pubs.acs.org/10.1021/acs.jpca.0c04917

Notes

The authors declare no competing financial interest.

ACKNOWLEDGMENTS

This work was funded by the National Science Foundation, award number CBET-1706825. Additional funding came from the TEES Turbomachinery Laboratory.

■ REFERENCES

- (1) Bond, E. J.; Robinson, J. R.; Buckland, C. T. The toxic action of phosphine: Absorption and symptoms of poisoning in insects. *J. Stored Prod. Res.* **1969**, *5*, 289–298.
- (2) Ohtani, H.; Horiguchi, S.; Urano, Y.; Iwasaka, M.; Tokuhashi, K.; Kondo, S. Flammability limits of arsine and phosphine. *Combust. Flame* **1989**, *76*, 307–310.
- (3) Buchan, N. I.; Jasinski, J. M. Calculation of unimolecular rate constants for common metalorganic vapor phase epitaxy precursors via RRKM theory. *J. Cryst. Growth* **1990**, *106*, 227–238.
- (4) Cardelino, B. H.; Moore, C. E.; Cardelino, C. A.; McCall, S. D.; Frazier, D. O.; Bachmann, K. J. Semiclassical calculation of reaction rate constants for homolytical dissociation reactions of interest in organometallic vapor-phase epitaxy (OMPE). *J. Phys. Chem. A* **2003**, 107, 3708–3718.
- (5) Bouvet, N.; Linteris, G. T.; Babushok, V. I.; Takahashi, F.; Katta, V. R.; Krämer, R. A comparison of the gas-phase fire retardant action of DMMP and Br₂ in co-flow diffusion flame extinguishment. *Combust. Flame* **2016**, *169*, 340–348.
- (6) Mathieu, O.; Kulatilaka, W. D.; Petersen, E. L. Shock-tube studies of Sarin surrogates. *Shock Waves* **2019**, *29*, 441–449.
- (7) Yu, X.; Li, S.-M.; Liu, J.-Y.; Xu, Z.-F.; Li, Z.-S.; Sun, C.-C. Direct dynamics study on the hydrogen abstraction reaction $PH_3 + H \rightarrow PH_2 + H_2$. *J. Phys. Chem. A* **1999**, *103*, 6402–6405.
- (8) Lee, J. H.; Michael, J. V.; Payne, W. A.; Whytock, D. A.; Stief, L. J. Absolute rate constant for the reaction of atomic hydrogen with phosphine over the temperature range 209 to 495 K. *J. Chem. Phys.* 1976, 65, 3280–3283.
- (9) Aleksandrov, E. N.; Arutyunov, V. S.; Dubrovina, I. V.; Kozlov, S. N. Reactions of hydrogen and oxygen atoms with phosphine: The role of PO radicals in the burning of phosphine. *Combust., Explos. Shock Waves* **1982**, *18*, 451–455.
- (10) Arthur, N. L.; Cooper, I. A. Arrhenius parameters for the reactions of H atoms with PH₃ and AsH₃. *J. Chem. Soc., Faraday Trans.* **1997**, 93, 521–524.
- (11) Mathieu, O.; Petersen, E. L. Experimental and modeling study on the high-temperature oxidation of ammonia and related NOx chemistry. *Combust. Flame* **2015**, *162*, 554–570.
- (12) Yi, H.; Yu, Q.; Tang, X.; Ning, P.; Yang, L.; Ye, Z.; Song, J. Phosphine adsorption removal from yellow phosphorus tail gas over CuO–ZnO–La₂O₃/activated carbon. *Ind. Eng. Chem. Res.* **2011**, *50*, 3960–3965.
- (13) Burcat, A.; Ruscic, B. Third millenium ideal gas and condensed phase thermochemical database for combustion; Report No. ANL-05/20 and TAE 960, Argonne National Lab: Argonne, IL, 2005.
- (14) Mulvihill, C. R.; Alturaifi, S. A.; Petersen, E. L. High-temperature He- and O_2 -broadening of the R(12) line in the 1 \leftarrow 0 band of carbon monoxide. *J. Quant. Spectrosc. Radiat. Transfer* **2018**, 217, 432–439.
- (15) Tarrago, G.; Lacome, N.; Lévy, A.; Guelachvili, G.; Bézard, B.; Drossart, P. Phosphine spectrum at 4–5 μ m: Analysis and line-by-line simulation of $2\nu_2$, ν_2 + ν_4 , $2\nu_4$, ν_1 , and ν_3 bands. *J. Mol. Spectrosc.* **1992**, 154, 30–42.
- (16) Gordon, I. E.; Rothman, L. S.; Hill, C.; Kochanov, R. V.; Tan, Y.; Bernath, P. F.; Birk, M.; Boudon, V.; Campargue, A.; Chance, K. V.; et al. The HITRAN2016 molecular spectroscopic database. *J. Quant. Spectrosc. Radiat. Transfer* **2017**, 203, 3–69.
- (17) Dhib, M.; Bouanich, J.-P.; Aroui, H.; Broquier, M. Collisional broadening coefficients in the ν_4 band of NH₃ perturbed by He and Ar. *J. Mol. Spectrosc.* **2000**, *202*, 83–88.

- (18) Cottrell, T. L.; Macfarlane, I. M.; Read, A. W.; Young, A. H. Measurement of vibrational relaxation times by the spectrophone. Application to CH₄, CO₂, N₂O, COS, NH₃ and HCN. *Trans. Faraday Soc.* **1966**, *62*, 2655–2666.
- (19) Tsang, W.; Hampson, R. F. Chemical kinetic data base for combustion chemistry. Part I. Methane and related compounds. *J. Phys. Chem. Ref. Data* **1986**, *15*, 1087–1279.
- (20) Holzrichter, K.; Wagner, H. G. G. On the thermal decomposition of ammonia behind shock waves. *Symp. (Int.) Combust., [Proc.]* **1981**, 18, 769–775.
- (21) Davidson, D. F.; Kohse-Höinghaus, K.; Chang, A. Y.; Hanson, R. K. A pyrolysis mechanism for ammonia. *Int. J. Chem. Kinet.* **1990**, 22, 513–535
- (22) Svehla, R.A. Estimated viscosities and thermal conductivities of gases at high temperatures; Report No. TR R-132, NASA: Cleveland, OH, 1962
- (23) Zhang, Y.; Mathieu, O.; Petersen, E. L.; Bourque, G.; Curran, H. J. Assessing the predictions of a NO_x kinetic mechanism on recent hydrogen and syngas experimental data. *Combust. Flame* **2017**, *182*, 122–141.